AIP | Review of Scientific Instruments

A cylindrically symmetric “micro-Mott” electron polarimeter

N. B. Clayburn, E. Brunkow, S. J. Burtwistle, G. H. Rutherford, and T. J. Gay

Citation: Review of Scientific Instruments **87**, 053302 (2016); doi: 10.1063/1.4946995

View online: http://dx.doi.org/10.1063/1.4946995

View Table of Contents: http://scitation.aip.org/content/aip/journal/rsi/87/5?ver=pdfcov

Published by the AIP Publishing

REVIEW OF SCIENTIFIC INSTRUMENTS **87**, 053302 (2016)

A cylindrically symmetric "micro-Mott" electron polarimeter

N. B. Clayburn,[1] E. Brunkow,[1] S. J. Burtwistle,[1] G. H. Rutherford,[2] and T. J. Gay[1]
[1]*Jorgensen Hall, University of Nebraska, Lincoln, Nebraska 68588-0299, USA*
[2]*Department of Physics, Illinois State University, Normal, Illinois 61790-4650, USA*

(Received 12 January 2016; accepted 2 April 2016; published online 6 May 2016)

A small, novel, cylindrically symmetric Mott electron polarimeter is described. The effective Sherman function, S_{eff}, or analyzing power, for 20 kV Au target bias with a 1.3 keV energy loss window is 0.16 ± 0.01, where uncertainty in the measurement is due primarily to uncertainty in the incident electron polarization. For an energy loss window of 0.5 keV, S_{eff} reaches its maximum value of 0.24 ± 0.02. The device's maximum efficiency, I/I_o, defined as the detected count rate divided by the incident particle rate, is $3.7 \pm 0.2 \times 10^{-4}$ at 20 keV. The figure-of-merit of the device, η, is defined as $S_{eff}^2 \frac{I}{I_o}$ and equals $9.0 \pm 1.6 \times 10^{-6}$. Potential sources of false asymmetries due to detector electronic asymmetry and beam misalignment have been investigated. The new polarimeter's performance is compared to published results for similar compact retarding-field Mott polarimeters, and it is concluded that this device has a relatively large S_{eff} and low efficiency. SIMION® electron trajectory simulations and Sherman function calculations are presented to explain the differences in performance between this device and previous designs. This design has an S_{eff} that is insensitive to spatial beam fluctuations and, for an energy loss window >0.5 keV, negligible background due to spurious ion and X-ray production at the target. *Published by AIP Publishing.* [http://dx.doi.org/10.1063/1.4946995]

I. INTRODUCTION

Spin-polarized electron experiments have made notable contributions to a variety of disciplines, including atomic and molecular physics,[1,2] high energy nuclear physics,[3,4] and solid state physics.[5–7] Electron polarimetry is often a crucial component of such experiments and Mott scattering is the most commonly used method.[8] In Mott polarimetry, electrons are typically scattered at energies between 10 keV and 5 MeV from high-Z target materials such as gold and thorium. The spin-orbit interaction in the scattering process yields a left-right asymmetry in the scattered electron signal measured at azimuthal scattering angles $\phi = \pm 90°$ to the transverse (with respect to the electron momenta) component of the spin polarization. The measured asymmetry for a given polar scattering angle $\boldsymbol{\theta}$ and incident electron energy E is

$$A(\theta, E) = \frac{N_L - N_R}{N_L + N_R}, \quad (1)$$

where N_L and N_R are the number of scattered electrons detected at azimuthal angles $\phi = -90°$ and $+90°$, respectively. If we assume no instrumental asymmetry, $A(\theta, E)$ is proportional to the beam polarization, i.e.,

$$A(\theta, E) = P S_{eff}(\theta, E), \quad (2)$$

where the analyzing power for the scattering, $S_{eff}(\theta, E)$, is called the "effective" Sherman function. The value of S_{eff} depends on the target material, polar scattering angle, incident electron energy, energy loss of the scattered electrons, and other geometric details of the device.

The design and characteristics of Mott electron polarimeters have been reviewed (see, e.g., Refs. 8–10). "Retarding-field" polarimeters, in which scattered electrons are decelerated prior to reaching the detector by the same field used for acceleration to the target scattering energy, incorporate of a pair of electrodes with either quasi-hemispherical[11] or cylindrical[12,13] symmetry. These serve to provide the accelerating/decelerating field for the incident electrons and also focusing for the incoming beam in the accelerating field. The geometry of these polarimeters causes inelastic scattering events to be electrostatically rejected, which eliminates the need for energy analysis by the electron detectors. In existing retarding-field designs, the high-Z target is contained within the inner electrode and is biased slightly negatively with respect to that electrode. This prevents positive ions sputtered from the target surface from being accelerated toward the detectors.[13] The detectors are placed just outside the outer electrode and held at or near the potential of that electrode.

We define the energy loss window, ΔE, as the largest energy loss that an electron can suffer and still be detected. The detector entrance potential and the kinetic energy of the incident electron beam determine ΔE. Generally speaking, S_{eff} increases and the detector count rate decreases with decreasing ΔE. One metric for a polarimeter's performance is its "figure of merit," $\eta = S_{eff}^2 \frac{I}{I_o}$, where I_o is the incident electron particle current and I is the detector count rate. This parameter is inversely proportional to the square of the time required to make a polarization measurement to a given statistical precision.[1]

Relatively simple and compact polarimeter designs are desirable in that they are easier and less expensive to fabricate and are easier to place and move about in a vacuum chamber. They also tend to have a high efficiency, I/I_o, and thus a high η. Retarding field designs are particularly suited to size reduction. So-called "micro-Motts" with compact quasi-hemispherical and conical designs have been developed to a high level of refinement,[9,11,14,15] but to our knowledge, compact *cylindrical* retarding field designs do not exist. This is due possibly to several assumptions that we will discuss below.

We report here a particularly simple, compact Mott polarimeter with cylindrical symmetry. Although its volume is ~1.8 times that of the smallest previous retarding-field "micro-Mott" device,[14] it is significantly simpler, incorporating a monolithic target structure and particularly simple detectors without entrance optics. Unlike conventional retarding-field Mott polarimeters, it does not have a double inner electrode structure. Instead it uses a single inner electrode that also serves as the target. Such a device was expected to exhibit at least two serious problems. First, unlike polarimeters with planar targets surrounded by the inner high-voltage electrode, it has been assumed that small fluctuations of the beam position on the combined target/inner electrode of the present device would result in large fluctuations in the detected asymmetry.[8] Similarly, it was expected that a small misalignment of the inner and outer electrode axes or of the input beam axis could result in a large instrumental asymmetry. Second, it was assumed that positive ions sputtered from the inner target electrode surface would reach the detectors and produce spurious background counts.

This paper describes the evaluation of our novel polarimeter, with particular attention being paid to these possible instrumental effects. We find experimentally that both are negligible above a certain energy window, ΔE, and propose a simple explanation for this, using computer simulations.

II. MOTT POLARIMETER DESIGN

Fig. 1 shows simplified views of the device. This polarimeter's compact, simple design allows for easy construction with basic machining tools, ideal for construction in a typical university student machine shop. The inner electrode is a solid 6.4 mm diameter copper rod. About 25 mm of its length near its vertical center has been electroplated with gold of thickness 1 μm, as measured with a precision mechanical stylus. The outer electrode is machined from a solid piece of aluminum and has an inner radius of 25 mm. The inner surface and the edges of the opening for beam entry and detector access are polished with a buffing compound suitable for aluminum (commonly called "white rouge") to inhibit electrical breakdown. The inner electrode is held in place by a machinable ceramic bar at each end. Each bar has been crenelated to suppress breakdown along its surface. The potential difference between the electrodes during normal operation is 20 kV, which is much less than the critical voltage at which electrical breakdown has been observed to occur, around 33 kV. The detectors are channel electron multipliers (CEMs) with conical mouths having entrance aperture diameters of 25 mm.[16]

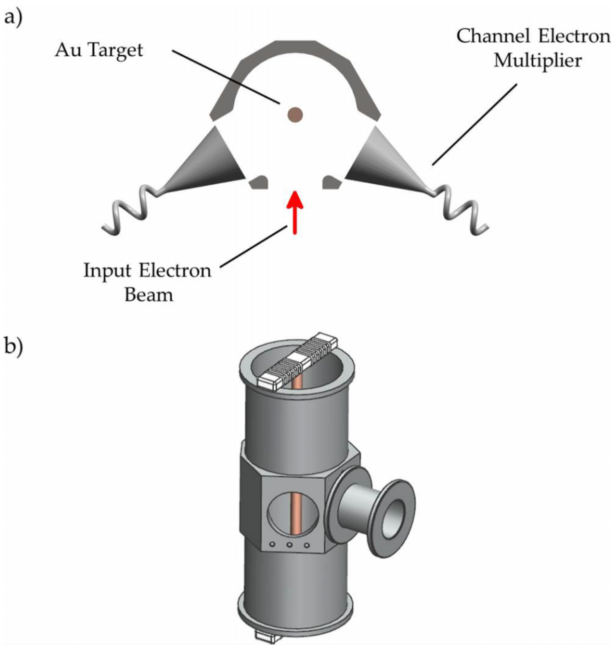

FIG. 1. Schematic top sectional (a) and isometric (b) views of the polarimeter. The channel electron multiplier detectors are not shown in (b).

Although the benefits of small size in such a device are considerable, some attention must be given to the electric field at the inner electrode surface. The electric field is largest at this surface and grows quickly as the electrode's radius is reduced. For concentric cylindrical electrodes with inner radius r_i, outer radius r_o, and a potential difference U, the electric field at the surface of the inner electrode is given by

$$E = \frac{U}{r_i \ln(\frac{r_o}{r_i})}, \qquad (3)$$

which, for a fixed U and r_o, is a minimum if $\frac{r_o}{r_i} = e$.[13] For our device $\frac{r_o}{r_i} = 8$, and the resulting electric field at the inner electrode surface is about 40% greater than the minimum possible value.

III. EFFICIENCY AND ASYMMETRY MEASUREMENT PROTOCOL

The polarized electron source we used to test the Mott polarimeter is based on photoemission from GaAs and is a modified version of that described in Ref. 12. It uses a 30 mW, 780 nm CW diode laser. The photocathode is biased at −200 V with respect to ground. The extracted beam is electrostatically bent by 90° to make it transversely polarized and then focused and steered into the Mott target chamber through a differentially pumped transport section containing a beam-defining 2 mm diameter aperture. A pair of magnetic dipoles just downstream from the aperture allow for further steering of the electron beam without effecting its polarization. The electron beam crosses the Mott vacuum chamber through an open, field-free region before entering the polarimeter. A movable flag just upstream of the Mott entrance was used to measure the position, diameter, and current of the incident beam. The beam's diameter was determined to be <2 mm at the flag. A single element serves as the polarimeter's entrance optic and is the only focusing element in the target chamber (Fig. 1(b)). This cylindrical "spool" electron entrance electrode can be floated, but in the current work it was held at the same voltage as the outer cylindrical electrode.

Polarized electron sources based on 780 nm photoemission from bulk ⟨110⟩ GaAs photocathodes that we have used in our lab, under quite similar vacuum conditions, typically have polarizations $P = 28\% \pm 2\%$.[17–20] Our polarization measurements of the present source using neon optical electron polarimetry[21] were consistent with the above value, and so we base our reported values of S_{eff} on this number. Although GaAs sources of this kind can have lower polarization, typically due to multiple resistive heat-cleanings of the photocathode,[22] we consider this a conservative estimate.

The parameters most often used to characterize a Mott polarimeter are its efficiency, I/I_o, effective Sherman function, S_{eff}, and figure of merit, $\eta = S_{eff}^2 \frac{I}{I_o}$. In order to ameliorate the effects of geometric instrumental asymmetries, differences in detector efficiencies, and spin-related beam intensity variations, the incident beam polarization was varied regularly during measurements. The experimental asymmetry is thus constructed as[8]

$$A = PS_{eff} = \frac{X-1}{X+1}, \tag{4}$$

where

$$X = \sqrt{\frac{R_L R'_R}{R_R R'_L}} \tag{5}$$

and the count rates R have subscripts indicating whether they correspond to the "right" or "left" detector, and the prime indicates one of the two incident spin states. Asymmetry measurements were made by accumulating counts from the detectors for 10 s, reversing the polarization, and reinitiating the data acquisition sequence. This cycle was repeated until sufficient counts were acquired such that the statistical error in A was less than 2% of its value. Background subtractions were made at uniform intervals during operation of the polarimeter by blocking the laser that caused GaAs photoemission. The background rate was <1% of the typical signal rate.

To ensure that a single CEM pulse was associated with a true target-scattered electron event and that dead time issues would not affect the result, the Mott polarimeter was operated in a regime where count rates increased linearly with incident beam current and I/I_o was constant. This occurred at count rates less than 100 kHz from target currents of ∼4 pA at 20 kV target bias. The CEMs were shown to be saturated by increasing their gain until the measured count rates began to plateau. The detector output signals were sent through amplifiers and discriminators placed near the target chamber.[23,24] Discriminator thresholds were set by optimizing signal-to-noise ratios.

The biases placed on the target, CEM cones, CEM back end, and the outer electrode were routinely varied in these measurements. The gold rod bias V_T was varied between 10 and 20 kV. The energy loss window, ΔE, was adjusted by varying the biases applied to the CEM cones. (Whenever the CEM cone biases were varied, the CEM bias voltage between the cone and collector was fixed.) The cones of the CEMs and the outer electrode were biased at the same voltage during normal operation, between 100 and 1100 V. This corresponds to a ΔE of between 300 and 1300 eV for 200 eV incident electrons. These ranges of ΔE and V_T values are common and allow for comparison of this device with other micro-Mott polarimeters.

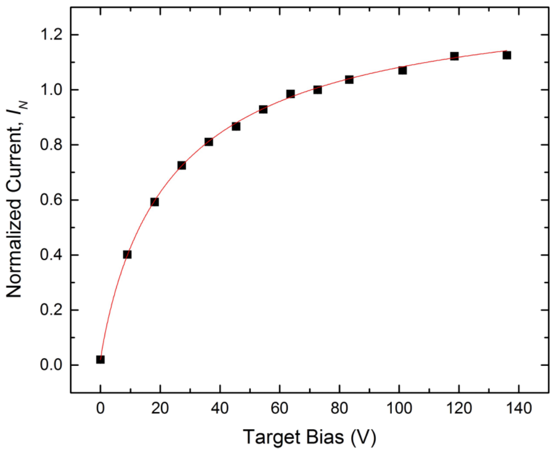

FIG. 2. Normalized target current, I_N, as a function of target bias, V_T, for a fixed incident electron beam current. The line indicates the fit curve (Eq. (6)) with A = 1.38, B = 1.36, C = 25.18 V, and D = 0.92.

The efficiency, I/I_o, was determined using the same polarized electron beam as that used for the asymmetry measurements. Ideally, measurements of the incident beam current, I_o, would be made by biasing the target at operating voltage and measuring the target current with an isolated picoammeter. This kind of measurement is complicated and can suffer from large systematic errors. Instead we measured I_o by biasing the target at 73 V with the CEM cones and outer electrode at ground and determining the beam current incident on the target with a case-ground picoammeter. (This voltage was near the maximum recommended voltage to which the picoammeter could be floated without isolation.) It was necessary to verify that the target current measured this way was substantially the same as that when the target was biased at high voltage, so target currents at higher biases were measured using batteries up to 136 V. Fig. 2 shows target currents normalized to the current measured at V_T = 73 V, I_N, as a function of target bias. These data were fit to the heuristic function

$$I_N = A - \frac{B}{(1+\frac{V_T}{C})^D}, \tag{6}$$

whose asymptote has zero slope as $V_T \rightarrow \infty$. This functional form satisfies the physical requirement that for very large biases, all of the incident current will strike the central rod and the measured current will not be diminished by secondary electron emission. Thus in our efficiency measurements, the value of I_o was obtained by multiplying the current measured with V_T = 73 V by A = 1.38. The target was then biased at high voltage and count rates corresponding to the scattered beam current, I, were measured.

Individual differences in the construction, handling, and operation of CEMs can lead to the same model having different electron detection efficiencies from unit to unit. It is reasonable to assume that we could replace the less sensitive CEM with one that is comparably efficient to the more sensitive CEM. We thus calculated the efficiency using a doubled count rate from the more sensitive CEM, to give a more realistic estimate of the achievable efficiency with CEMs of this type.

The experimental asymmetry (and thus the effective Sherman function; Eqs. (4) and (5)) is not dependent on the difference in detector efficiencies owing to its algebraic construction (see Eqs. (13)-(17), Ref. 8). The error associated with these quantities, however, is dependent on the difference in detector efficiencies. An order of magnitude difference in count rates between the two detectors due to differing efficiencies, as compared to identical counts rates, results in a ~2.5 times larger statistical counting error in the asymmetry.

The backscattered electron signal can be contaminated by positive ions sputtered from the target surface and from X-rays generated in the scattering process. To determine the combined contribution of these, count rates during normal operation and count rates due only to the summed positive ion and X-ray contributions were compared. The combined positive ion and X-ray count rate was measured by biasing the entrance cathodes of the CEMs such that electrons scattered from the rod had insufficient energy to surmount the potential barrier in front of them. It was concluded that 7% of the total rate observed during normal operation (ΔE = 300 eV, V_T = 20 kV) was due to either positive ions or X-rays. Detection of positive ions sputtered from the high-voltage rod and X-rays was not significantly affected by outer electrode potentials ranging from 100 to 1100 V, so the number of X-rays and positive ions remained constant as a function of ΔE. However, the detected electron rate increases drastically as a function of ΔE, and so the contamination percentage decreases with increasing ΔE. Given the contribution of positive ions and X-rays at ΔE = 300 V, we estimate that 0.02% of the total count rate at ΔE = 1300 eV is due to positive ion and X-ray contributions.

These results are supported and supplemented by simulated electron and ion trajectory analysis using SIMION.[25] A 3D model of the Mott polarimeter was constructed to examine the effects of the biases applied to the apparatus. In order to simulate the behavior of electrons scattered from the target rod (V_T = 20 keV), we first determined the spot size on the rod of the electron beam. (The incident beam had cylindrical symmetry, a kinetic energy of 200 eV, and a diameter of 2 mm.) At ΔE = 1300 eV, the simulated beam spot on target extended 2.46 mm along the rod axis, with a perpendicular width of 0.84 mm. The large aspect ratio, defined as the beam's parallel extent divided by its perpendicular extent, is due to the strong one-dimensional radial focusing the electron beam undergoes. At or above ΔE = 500 eV, the aspect ratio ranged from 25 at 500 eV to 3 at 1300 eV. The aspect ratio is much smaller at lower ΔE. At ΔE = 300 eV, the beam spot measured 0.38 mm along the rod axis and 0.3 mm perpendicular to it. The tightest perpendicular focusing occurred at ΔE = 500 eV (0.04 mm), and the tightest parallel focusing at ΔE = 200 eV (0.01 mm).

For these experiments, the polarimeter entrance cylinder was held at the same potential as the CEM cones and outer electrode. This was done to create a more uniform electrostatic environment for the scattered electrons. In principle, the entrance aperture could have been held at a different potential than that of the CEM cones. The entrance aperture effectively behaved as a single lens element. Changing ΔE by adjusting the CEM entrance cone bias (and thus changing the entrance aperture voltage) caused a change in the input beam electrostatic focusing at the polarimeter entrance. This in turn caused the spot size to vary even with fixed V_T = 20 kV.

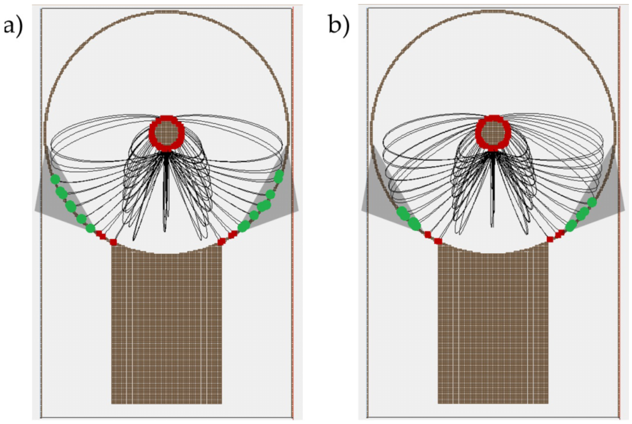

FIG. 3. Simulated trajectories for electrons scattered from the 20 kV target having either lost (a) 0 eV or (b) 500 eV of kinetic energy in the collision. The shaded triangular regions denote the location of the CEM detector's front-end cones. The trajectories ending with green circles correspond to detected events which comprise the detected scattered electron fraction shown in Fig. 4. The red squares indicate the termination of trajectories that were not detected. The trajectories shown originate from the spot where the incident electron beam strikes the rod target and correspond to scattering angles between 115° and 155°. The input electron beam is not shown. For reference, it would enter vertically from the bottom of the figure and its direction of propagation defines the 0° scattering angle. The outer electrode potential is 1100 V.

The simulated trajectories of electrons emerging from the target, with an energy distribution corresponding to both elastically and inelastically scattered electrons from thick Au targets,[26] were examined to determine if those electrons would reach the CEMs (Fig. 3). Particles were considered to be detected if their trajectories terminated (noted by green squares) inside the area subtended by the CEMs (noted by the triangular shaded regions). The emerging particles were assumed to be emitted isotropically into the backward hemisphere centered on the target focal spot. This distribution, assuming single scattering only, approximates the calculated differential cross section for Mott scattering of electrons by screened Au nuclei.[27] The fraction of scattered electrons that reached the CEMs was determined for various outer electrode voltages (Fig. 4). This analysis showed a rapid monotonic decrease with ΔE of the fraction of scattered electrons arriving at the CEMs, due entirely to electrostatic effects. The behavior of the experimental efficiency I/I_o on a fractional basis is qualitatively similar. Our studies of X-ray and ion contamination in conjunction with these electrostatic simulations suggest that measurements with $\Delta E < 500$ eV are not ideal.

Simulations, like those described above, using a concentric spherical Mott geometry with equivalent radii were also conducted. The simulated target was a small sphere. Two times as many scattered electrons were delivered to the detectors with this geometry compared with our cylindrical system. We attribute this increase to two-dimensional spherical focusing.

The SIMION simulations also suggest that almost no positive ions reach the CEM detectors (Fig. 5). Calculated trajectories for H^+, N^+, O^+, O_2^+, N_2^+, Au^+, Au^{++}, and Au^{+++} ions originating from the 20 kV target with zero initial kinetic energy fail to reach the CEM detectors because of the strong one-dimensional radial focusing. The ions originated at the

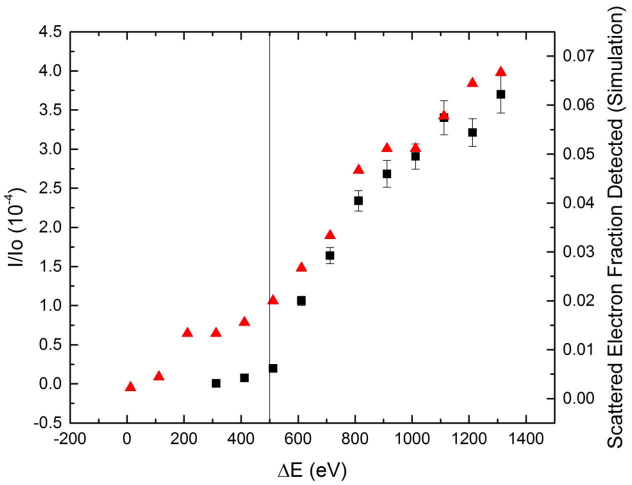

FIG. 4. Efficiency, I/I_o (squares), and the fraction of simulated electrons (triangles) which reach the CEMs as a function of ΔE. Note that both quantities have similar functional dependence. The increase of efficiency above 500 V is due to the enhanced acceptance of inelastically scattered electrons, which has been accounted for in the SIMION simulations.

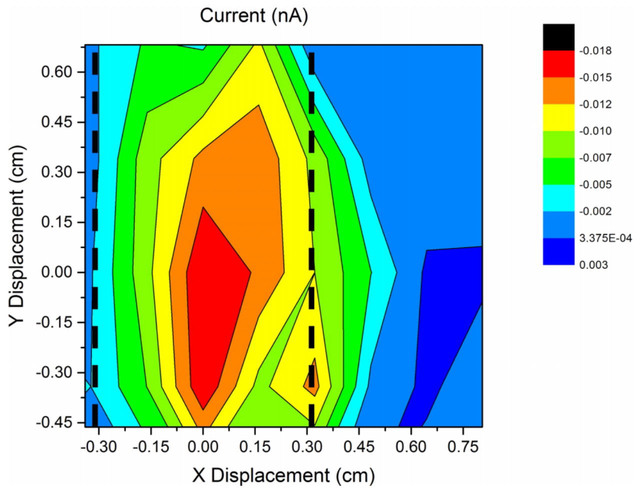

FIG. 6. Variation of the beam current measured on the target rod when it is held at $V_T = +73$ V. The x- and y-displacements are calculated at the entrance of the polarimeter assuming no focusing effects due to the voltage on the entrance electrode. The origin of the displacement coordinate system corresponds to no magnetic dipole steering. The indicated current scale is linear but otherwise arbitrary. The target rod width extends from x = −0.32 cm to x = +0.32 cm (denoted by dashed lines).

electron beam focal spot on the target and their trajectories were followed for various outer electrode voltages. It was not until the electrons imparted to the nascent ions almost 4%-6% of their kinetic energy that the ions reached the detectors in the simulation. Such efficient energy transfer between electrons and ions is unlikely. We conclude that the small non-electron signal reported above must be predominantly due to X-rays.

IV. INSTRUMENTAL ASYMMETRIES

The dependence of S_{eff} on beam misalignment has been explored by purposely misaligning the electron beam using a set of magnetic dipoles upstream of the polarimeter chamber. The target current (measured at $V_T = 73$ V) is shown as a function of the x- and y-displacement produced by the upstream steering elements (Fig. 6). The maximum current is observed in the region of no upstream steering (x = y = 0), indicating good alignment of the apparatus. We note that with only weak electrostatic attraction by the rod, the beam spot is still well localized and is qualitatively similar to what we expect from our SIMION predictions.

Fig. 7 shows the effect of beam steering on the value of S_{eff} when the target voltage V_T is now increased to its nominal operating value of 20 kV, with ΔE = 1300 eV. We now expect the beam's focal spot on target to be 2.46 mm (along the target axis) by 0.04 mm (perpendicular to it). The S_{eff} value does not change, within statistical uncertainty, over a very large steering range. This indicates that despite its compact size and non-optimal focusing, the polarimeter is stable against spurious spatial beam fluctuations.

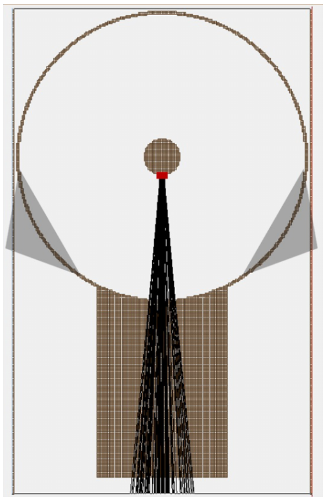

FIG. 5. Simulated trajectories for 0 eV O^+ ion sputtered from the target. The shaded triangular regions denote the location of the CEM front-end cones. The target potential V_T is 20 kV, and the outer electrode potential is 1100 V. The red squares identify the region where the ions trajectories originate.

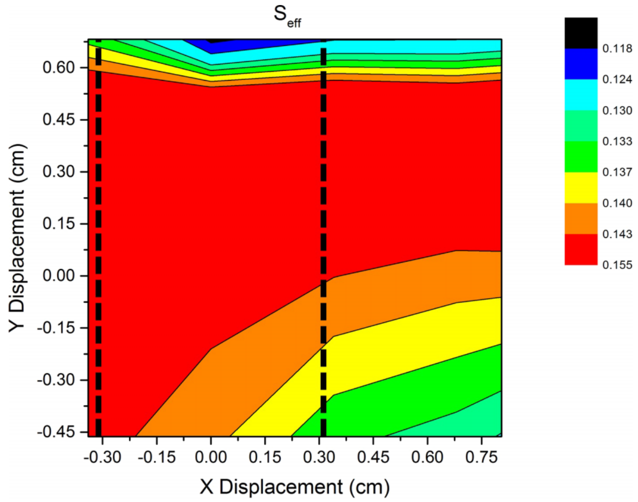

FIG. 7. Variation of S_{eff} as a function of electron beam displacement at the polarimeter entrance for 20 kV target bias and ΔE = 1300 eV. The target rod width extends from x = −0.32 cm to x = +0.32 cm (denoted by dashed lines).

Typically, the ratio between left and right detector count rates was approximately 6. The results of Figs. 6 and 7 show that this is not due to severe beam misalignment. It is instead due to differences in left-right detector efficiency. This ratio was purposely varied by adjusting the voltage difference across one of the CEMs, causing the ratio to vary from 5 to 7. (This was the largest variation in the ratio of count rates we could attain and still operate in the appropriate plateau region of both detectors.) The value of S_{eff} was then measured and shown to remain constant as a function of this left and right count rate ratio. This is another indication of the robustness of the cross-ratio method described earlier.

V. RESULTS

Values of S_{eff}, I/I_o, and η with the largest ΔE of 1300 eV are shown as a function of V_T in Fig. 8. (The ΔE of 1300 eV was chosen so that comparisons with other polarimeters could be made most readily.[11,28]) The monotonic decrease of I/I_o with increasing target voltage is the result of lowered electron scattering cross section at higher incident energies. The S_{eff} for $V_T = 20$ kV with $\Delta E = 1300$ eV is 0.156 ± 0.001 (stat.) $\pm$ 0.011(syst.). Our systematic error is due primarily to uncertainty in the polarization of the incident electrons.

Values of S_{eff}, I/I_o, and η as a function of ΔE are shown in Fig. 9 for $V_T = 20$ kV. An increase in I/I_o at the expense of a decreasing S_{eff} is observed as a function of increasing energy loss window for $\Delta E \geq 500$ eV. Below 500 eV, the increasing relative contribution from X-rays reduces S_{eff}. The maximum value of S_{eff} that we observe occurs at $\Delta E = 500$ eV, and equals 0.239 ± 0.007 (stat.) $\pm$ 0.017 (syst.). We note that due to the increasing relative importance of X-ray background as energy loss rejection becomes more complete, our S_{eff} values are not monotonically decreasing with increasing ΔE. This is in contrast with the reports of other investigators.[9,14,29] However, Ref. 29 only reports values of S_{eff} for $\Delta E > 500$ eV. This effect also accounts for the strong ΔE dependence of η and I/I_o below 700 eV (Figs. 9(b) and 9(c)).

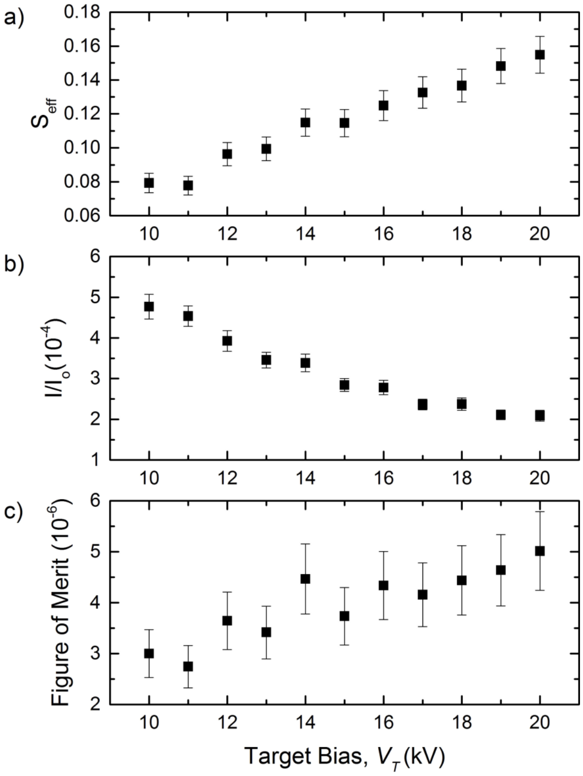

FIG. 8. Variation as a function of target bias of (a) the effective Sherman function, S_{eff}, (b) efficiency, I/I_o, and (c) figure of merit, η, for the Mott polarimeter. The incident electron energy was 200 eV and ΔE = 1300 eV.

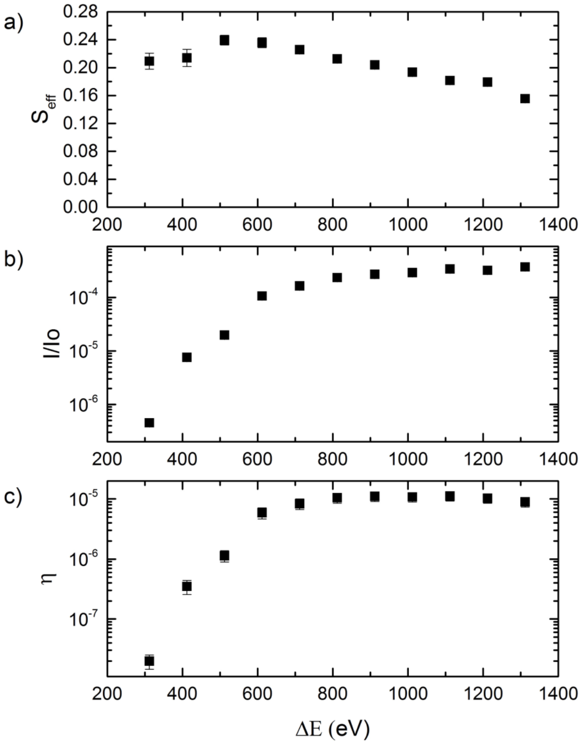

FIG. 9. Variation as a function of ΔE of (a) the effective Sherman function, S_{eff}, (b) efficiency, I/I_o, and (c) figure of merit, η. The incident electron energy was 200 eV with a target bias of 20 kV.

VI. CONCLUSIONS

At the beginning of this study, we naively expected that the Mott polarimeter discussed in this report would have a generally high efficiency, perhaps at the expense of S_{eff}, due to its small size (the proximity of the detector to the target) and large detector solid angle. The opposite is true: Table I compares the operating characteristics of various "micro-Mott" polarimeters reported in the literature.[9]

The measured value for S_{eff} is about 1.4 times that of quasi-hemispherical polarimeters with similar accelerating voltages (20 kV), energy loss windows (1300 eV), gold targets, and detector solid angles.[12,28] These polarimeters have efficiencies roughly 6 times greater than ours. This difference in efficiency is due, in part, to the one-dimensional focusing of our cylindrical device, as opposed to the two-dimensional focusing of quasi-spherical micro-Mott polarimeters.

We note that the method for measuring the incident current I_o varies between reports. Some use procedures similar to those discussed here,[28] while others insert a Faraday cup

TABLE I. Comparison of various "micro-Mott" designs at 20 kV with Au, Th, and U targets. To facilitate comparison between our Au target polarimeter and devices that used Th targets, we have scaled S_{eff}, I/I_o, and η of our polarimeter using the method described in Ref. 9. The adjusted values are presented in the last row of the table.

References	Laboratory	Max. S_{eff} (%)	ΔE (eV)	Max. I/I_0 (10^{-4})	ΔE (eV)	S_{eff} at max. I/I_0 (%)	Max. η (10^{-5})	ΔE (eV)	S_{eff} at max. η (%)	ΔΩ (sr)	Volume (10^3 cm^3)	Notes
[14]	Rice	23	400	53	1000	16	13	400	23	0.21	1.1	[a]
[31]	Rice	21	300	94	1500	9	12	700	15	0.25	2.9	[b]
[12]	Rice	11	1300	~20	1300	11	2.4	1300	11	0.11	2.0	
[28]	Rice	11	1300	22	1300	11	2.7	1300	11	0.09	4.2	
[32]	Irvine	20	500	6.7	1000	14	1.4	1000	14			[c]
[33]	Taiwan	13	700				~2			0.60		[d]
[34]	Tokyo	13	600	195	1400	10	18	1200	10	0.57	1.2	
[35]	St. Petersburg						4.5			0.06	1.3	[e]
[36]	Edinburgh	9	1300							0.06	2.2	
[9]	JLab	20	0	5.4	268	13.5	1	268	14	0.27	1.4	
This work	Lincoln	24	500	3.7	1300	15.6	1.1	1100	18	0.86	2.0	
This work Th adj.	Lincoln	29	500	4.2	1300	17.4	1.7	1100	21	0.86	2.0	

[a] Th target 25 keV, max η occurs over range of ΔE from 400 to 1000 eV.
[b] Th target.
[c] U target.
[d] 23 keV.
[e] 30 keV; Refs. 14 and 31 indicate little change in η between 20 and 25 keV at 1300 eV.

into the incident beam path.[30] Still others have used dedicated electron guns close to the polarimeter's entrance (rather than the electron beam used to make the asymmetry measurement) to determine values of I/I_o.[14] Methods which measure I at the entrance of the polarimeter, as opposed to the current that reaches the scattering target, are more conservative.

As discussed in Section III, our polarimeter is significantly less efficient at ΔE = 300 eV than at ΔE = 1300 eV (Fig. 9), primarily due to geometric electrostatic issues. Even at ΔE = 1300 eV, when compared with other devices, the generally poor overall efficiency but large S_{eff} of our device was unexpected. These results can be understood by considering the specific scattered electron population we detect (Fig. 10). Conventional retarding-field Mott polarimeters detect electrons emitted from the electrostatic center of the polarimeter which follow almost perfectly radial paths. This polarimeter instead detects scattered electrons whose initial trajectories correspond to relatively large scattering angles that follow only quasi-radial paths, as shown in Figs. 3(a) and 3(b).

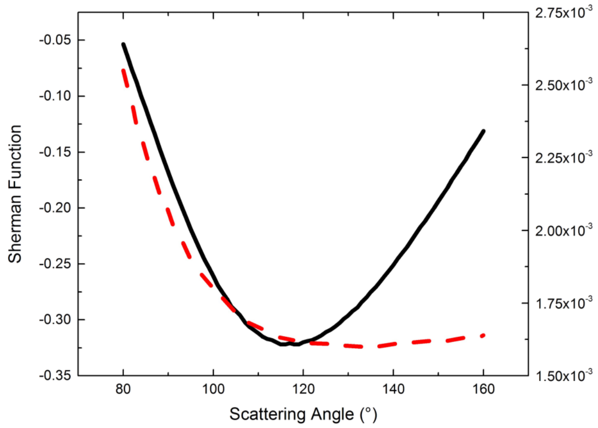

FIG. 10. Calculated Sherman function (solid line) and differential scattering cross section (dashed line) as a function of polar scattering angle.[27]

Our polarimeter's detectors subtend polar scattering angles of 20° and are centered at 120°, but unlike a conventional Mott polarimeter that would examine an electron population centered about 120°, our device detects electrons originating from higher-angle scattering. For the energy range in question, calculations[27] suggest that electrons scattered to these higher scattering angles have a greater absolute S_{eff} and a smaller scattering cross section (Fig. 10). Specifically, Fig. 10 shows that the Sherman function magnitude is maximized near 120° and that it drops off more slowly for θ > 120° than at lower scattering angles. Conversely, Fig. 10 shows that the cross section (proportional to the efficiency) is relatively low at higher scattering angles but rises quickly with decreasing scattering angle beneath about 120°. We speculate that the generally poor overall efficiency and generally large S_{eff} of this device is because it detects this higher-scattering-angle electron population.

ACKNOWLEDGMENTS

This work was funded by the National Science Foundation through Grants No. PHY-206067 and PHY 1505794 and by a Cottrell College Science Award from the Research Corporation. We would like to acknowledge the work of several undergraduate students at ISU: R. M. King for early design work and G. G. Shepard and M. S. Zimmerle for initial characterization of the device. The craftsmanship of J. U. Dunham (ISU) and the University of Nebraska Physics and Astronomy instrument shop was an essential part of this project.

[1] J. Kessler, *Polarized Electrons*, 2nd ed. (Springer, Berlin, 1985).
[2] T. J. Gay, Adv. At. Mol. Phys. **57**, 157 (2009).
[3] See, e.g., C. Y. Prescott *et al.*, Phys. Lett. B **77**, 347 (1978).
[4] See, e.g., D. Androic *et al.*, Phys. Rev. Lett. **111**, 141803 (2013), and references therein.
[5] See, e.g., *Polarized Electrons in Surface Physics*, edited by R. Feder (World Scientific, Singapore, 1985).
[6] See e.g., K. von Bergmann, M. Bode, A. Kubetzka, M. Heide, S. Blügel, and R. Wiesendanger, Phys. Rev. Lett. **92**, 046801 (2014).

[7] See e.g., F. Giebels, H. Gollisch, and R. Feder, Phys. Rev. B **87**, 035124 (2013).

[8] T. J. Gay and F. B. Dunning, Rev. Sci. Instrum. **63**, 1635 (1992).

[9] J. L. McCarter, M. L. Stutzman, K. W. Trantham, T. G. Anderson, A. M. Cook, and T. J. Gay, Nucl. Instrum. Methods Phys. Res., Sect. A **618**, 30 (2010).

[10] See, e.g., F. B. Dunning, Nucl. Instrum. Methods Phys. Res., Sect. A **347**, 152 (1994).

[11] F.-C. Tang, X. Zhang, F. B. Dunning, and G. K. Walters, Rev. Sci. Instrum. **59**, 504 (1988).

[12] See, e.g., T. J. Gay, M. A. Khakoo, J. A. Brand, J. E. Furst, W. V. Meyer, W. M. K. P. Wijayaratna, and F. B. Dunning, Rev. Sci. Instrum. **63**, 114 (1992).

[13] L. A. Hodge, F. B. Dunning, and G. K. Walters, Rev. Sci. Instrum. **50**, 1 (1979).

[14] D. D. Neufeld, H. Aliabadi, and F. B. Dunning, Rev. Sci. Instrum. **78**, 025107 (2007).

[15] F. B. Dunning, F.-C. Tang, and G. K. Walters, Rev. Sci. Instrum. **58**, 2195 (1987).

[16] Model 463, Detector Technology, Inc.

[17] B. G. Birdsey, H. M. Al-Khateeb, M. E. Johnston, T. C. Bowen, T. J. Gay, V. Zeman, and K. Bartschat, Phys. Rev. A **60**, 1046 (1999).

[18] J. M. Dreiling and T. J. Gay, Phys. Rev. Lett. **113**, 118103 (2014).

[19] J. E. Furst, W. M. K. P. Wijayaratna, D. H. Madison, and T. J. Gay, Phys. Rev. A **47**, 3775 (1993).

[20] J. W. Maseberg and T. J. Gay, Phys. Rev. A **79**, 022705 (2009).

[21] T. J. Gay, J. E. Furst, K. W. Trantham, and W. M. K. P. Wijayaratna, Phys. Rev. A **53**, 1623 (1996).

[22] J. W. Maseberg and T. J. Gay, J. Phys. B **39**, 4861 (2006).

[23] Ortec VT120C Pre-amplifier.

[24] Philips 6930 Discriminator.

[25] SIMION 8.1, Scientific Instrument Services, Inc.

[26] E. H. Darlington, J. Phys. D: Appl. Phys. **8**, 85 (1975).

[27] G. Holzwarth and H. J. Meister, Nucl. Phys. **59**, 56 (1964).

[28] F. B. Dunning, L. G. Gray, J. M. Ratliff, F.-C. Tang, X. Zhang, and G. K. Walters, Rev. Sci. Instrum. **58**, 1706 (1987).

[29] D. M. Oro, W. H. Butler, F.-C. Tang, G. K. Walters, and F. B. Dunning, Rev. Sci. Instrum. **62**, 667 (1991).

[30] L. G. Gray, M. W. Hart, F. B. Dunning, and G. K. Walters, Rev. Sci. Instrum. **55**, 88 (1984).

[31] G. C. Burnett, T. J. Monroe, and F. B. Dunning, Rev. Sci. Instrum. **65**, 1893 (1994).

[32] D. P. Pappas and H. Hopster, Rev. Sci. Instrum. **60**, 3068 (1989).

[33] D. J. Huang, W. P. Wu, J. Chen, C. F. Chang, S. C. Chung, M. Yuri, H.-J. Lin, P. D. Johnson, and C. T. Chen, Rev. Sci. Instrum. **73**, 3778 (2002).

[34] S. Qiao, A. Kimura, A. Harasawa, M. Sawada, J.-G. Chung, and A. Kakizaki, Rev. Sci. Instrum. **68**, 4390 (1997).

[35] V. N. Petrov, M. S. Galaktionov, and A. S. Kamochkin, Rev. Sci. Instrum. **72**, 3728 (2001).

[36] F. Ciccacci, S. De Rossi, and D. M. Campbell, Rev. Sci. Instrum. **66**, 4161 (1995).